Multilayer properties of superficial and intergranular segregation isotherms: A mean-field approach

Fabienne Berthier, Jérôme Creuze, and Robert Tétot
LEMHE, Université de Paris XI, F91405 Orsay Cedex, France

Bernard Legrand
SRMP-DMN, CEA Saclay, F91191 Gif-sur-Yvette Cedex, France
(Received 5 December 2001; published 29 April 2002)

Segregation is studied at the (001) and (310) surfaces, as well as for the $\Sigma=5$ (310) [001] tilt grain boundary (GB), in the Cu(Ag) system. Based on an effective Ising model with energetic parameters obtained from an *N*-body interatomic potential, we compare the segregation driving forces for the three interfaces in this system, which presents a strong tendency toward phase separation in the bulk. Within mean-field theory, we derive segregation isotherms, and we find an essential difference between the flat (001) surface and the open (310) surface. For the first one, the isotherm is characterized by a succession of monolayer phase transitions, whereas the isotherm of the (310) surface exhibits a multilayer phase transition, all these transitions occurring well within the domain of the Cu(Ag) solid solution. The segregation isotherm for the (310) [001] tilt grain boundary is similar to the (310) surface one, with the presence of a multilayer phase transition too. The behavior of the GB plane itself is rather intricate, a multireentrant phase transition being predicted. A ground-state analysis and a simple bilayer model allows us to detail the conditions for the existence of an interfacial multilayer phase transition, as a function of both the energetic and crystallographic parameters and the temperature.

DOI: 10.1103/PhysRevB.65.195413 PACS number(s): 68.35.Rh, 82.65.+r, 02.70.Rr

I. INTRODUCTION

The chemical composition in alloys near interfaces is in general different from that of the bulk. This phenomenon has been extensively studied for many years both for surfaces[1–3] and grain boundaries (GB's).[2,4–6] Atomic resolution experimental techniques now allow a more detailed comparison with atomistic simulations for both types of interface.[7–10] From a theoretical point of view, surface segregation has been modeled both analytically[3,11] and by numerical simulations such as the Monte Carlo technique.[12] The advantages of the first approach are obviously to allow one to extract the segregation driving forces and to study extensively the influence of physical parameters such as the bulk concentration or the temperature.[3] However, the rigid-lattice approximation, which is often assumed in the analytical approach,[11] neglects the influence of atomic relaxations. When the atomic radii of the elements of the alloy differ strongly, this approximation is probably too severe.[3,13,14] Conversely, Monte Carlo simulations coupling atomic displacements and a change of the chemical nature of the atoms include all factors that may induce superficial segregation.[12] However, due to their numerical aspect, these calculations are unsuited to derive trends in superficial segregation behavior. The same dilemma exists for the study of grain boundary segregation, but the large distortions of the interatomic distances between GB sites seem to prevent the use of simple lattice-gas models,[15–20] like those used for the surface case. This explains the large use of Monte Carlo simulations for GB segregation study,[21–24] and thus the lack of knowledge about the general trends followed by GB segregation isotherms, that are defined as the relation giving the concentration on each GB site as a function of the bulk concentration for a given temperature. In particular, first-order phase transitions such as the ones derived from the Fowler-Guggenheim surface isotherms[3,25] have not been reported for GB isotherms to the best of our knowledge.

Very recently, we extended the tight-binding Ising model (TBIM), developed for the study of surface segregation,[3,26] to the GB case.[27] The key point of this approach is that the energetic parameters of the Ising model are obtained from atomistic simulations using interatomic potentials derived from the second-moment approximation (SMA) of the tight-binding scheme.[28] This SMA-TBIM approach permits one to takes into account the influence of the atomic relaxations at the surface or in the GB zone and the variation of the width of the local density of electronic states on each site of the interface. Consequently, the energetic parameters of the effective Ising model are different for each site or for each pair of neighboring sites of an interface. It is obvious that such variations can strongly affect a segregation isotherm. In particular, it is an open question to know if it can induce specific interfacial phase transitions.

The goal of the present paper is to compare surface and GB segregation isotherms by taking advantage of the analytical properties of the SMA-TBIM approach. The Cu-Ag system is chosen due to the large number of studies on surface[27,29–35] and grain boundary[27,36–42] segregation. Segregation isotherms for the symmetrical tilt grain boundary $\Sigma=5$ (310) [001] will then be compared with two surface isotherms. The first one concerns the (001) low-index orientation, whereas the second one is related to the same orientation as the GB, i.e., the (310) surface. This will allow us to distinguish the respective roles of the nature of the interface (surface or GB) and its crystallographic orientation. Moreover, it seems that this is one of the first theoretical studies of

surface segregation for an open orientation, such as the (310) one, and we hope that the present results will motivate experimental studies on segregation at vicinal surfaces.

The paper is organized as follows. In Sec. II, we review the main features of the SMA-TBIM approach. In Sec. III, the values of the energetic parameters of the model are given for the (001) and (310) surfaces and for the $\Sigma=5$ (310) [001] GB for the Cu(Ag) system. Then the segregation isotherms are presented for all these interfaces, with special attention paid to possible interfacial phase transitions (Sec. IV). Some simple analytical models are presented in Sec. V to interpret the main differences observed between the phase transitions for the (001) surface, on the one hand, and the (310) interfaces (GB and surface), on the other hand. Then a quantitative comparison of the results of these simple analytical models with the isotherms obtained with the SMA-TBIM approach is performed in Sec. VI. Finally, in Sec. VII we list the general conclusions.

II. SMA-TBIM APPROACH

Let us recall the main features of the SMA-TBIM approach for studying surface and GB segregation.[3,27] Starting from the tight-binding Hamiltonian and using a generalized perturbation method, an effective Ising Hamiltonian is obtained to model the part of the energy that depends on the chemical configuration, which governs interfacial segregation.[3] The Bragg-Williams approximation is used for the statistical treatment. Moreover, we assume that the concentration is homogeneous for each plane parallel to the interface, at least when all the sites in such a plane are crystallographically equivalent. In the opposite case, we consider sublattices formed by equivalent sites, and we define a concentration per sublattice for each plane parallel to the interface. As shown below, this is the case for the (310) GB plane. However, for the sake of simplicity, we omit the index of the possible sublattices in the following equations and we denote c_p the concentration of A in the pth plane, $p=0$ being the interface plane.

The segregation isotherm for an A_cB_{1-c} alloy at temperature T is given by[3]

$$\frac{c_p}{1-c_p}=\frac{c}{1-c}\exp\left[-\frac{\Delta G_p^{seg}(c,c_p,c_{p'})}{k_BT}\right], \tag{1}$$

where $\Delta G_p^{seg}=\Delta H_p^{seg}-T\Delta S_p^{seg}$ is the Gibbs free energy of segregation on the pth plane; ΔH_p^{seg} and ΔS_p^{seg} being, respectively, the segregation enthalpy and the vibrational part of the segregation entropy on the pth plane. Each thermodynamic quantity ΔX_p^{seg}, with $X=(G,H,\text{or } S)$ corresponds to the variation of X when one A atom in the bulk is exchanged with a B atom in the pth plane parallel to the interface.

It has been shown that ΔH_p^{seg} may be expressed as[3,27,42]

$$\Delta H_p^{seg}(c,c_p,c_{p'})=\Delta H_p^{impurity}+\Delta H_p^{interaction}(c,c_p,c_{p'}), \tag{2}$$

where $\Delta H_p^{impurity}$ is the segregation enthalpy in the infinitely dilute limit and $\Delta H_p^{interaction}$ takes into account the interactions among segregating atoms,[27,42]

$$\Delta H_p^{interaction}(c,c_p,c_{p'})=2\sum_R\left(\sum_{p'=-q}^{p'=+q}Z_R^{p,p+p'}V_R^{p,p+p'}c_{p+p'}-Z_RV_Rc\right), \tag{3}$$

where $V_R=(V_R^{AA}+V_R^{BB}-2V_R^{AB})/2$ is the effective pair interaction energy (EPI) between the Rth neighbors.[43] Z_R is the bulk coordination number for the Rth shell of neighbors, and $Z_R^{p,p+p'}$ is the number of Rth neighbors between planes p and $p+p'$. The index q defines the number of planes that have to be considered ($2q+1$ in the bulk), consistently with the spatial extension of V_R. The EPI's can vary near the interface, which explains the occurrence of the exponent in $V_R^{p,p+p'}$ in the term that depends on $c_{p+p'}$.[3,44–46]

The segregation enthalpy in the infinitely dilute limit is the sum of three terms,[3,27,42]

$$\Delta H_p^{impurity}=\Delta H_p^{site}+\Delta H_p^{size}+\Delta H_p^{EPI}, \tag{4}$$

where ΔH_p^{site} is equal to the difference of the excess enthalpies of sites on the pth plane between the pure constituents,[3] and ΔH_p^{size} is the component of the segregation enthalpy due to the size mismatch between A and B.[3,14] The last term in Eq. (4) is related to the EPI's V_R (Ref. 47):

$$\Delta H_p^{EPI}=\sum_R V_R\left(Z_R-\sum_{p'=-q}^{p'=+q}Z_R^{p,p+p'}\right). \tag{5}$$

The key point of the SMA-TBIM approach is the possibility to calculate the energetic parameters of Eqs. (2)–(5) from realistic simulations.[27,42] This is performed using N-body interatomic potentials derived from the second-moment approximation of the tight-binding scheme.[28,42] The calculation of the excess enthalpy on each site in the pure metals, necessary to obtain ΔH_p^{site}, is obtained after minimizing the enthalpy with respect to atomic positions by means of a quenched molecular dynamics algorithm.[48] For the calculation of the size effect contribution ΔH_p^{size}, the parameters of the interatomic potentials are the same for the $A-A$, $A-B$, and $B-B$ interactions, except the one fixing the lattice parameter for each metal.[3,14] This procedure allows us to separate the size effect from both the site and EPI contributions for interfacial segregation. Finally, the bulk EPI's V_R are obtained by considering the enthalpy difference ΔH_R of a relaxed system containing two isolated solute atoms (initial state) and two solute atoms in Rth neighbor position (final state). V_R is related to ΔH_R by $V_R=\Delta H_R/2$.[42] Similar calculations are performed between the different sites of the interfaces to obtain $V_R^{p,p+p'}$, i.e., the values of the EPI's near the interfaces.

The vibrational part of the segregation entropy in Eq. (1), ΔS_p^{seg}, can be estimated by a recursion method,[49] using the relaxed values of the atomic positions and the force constants derived from the SMA potential. Previous work[41] showed that both the harmonic approximation and local Einstein model[50] are clearly too rough to predict the segregation entropy at the surface or in the GB quantitatively. Our results,

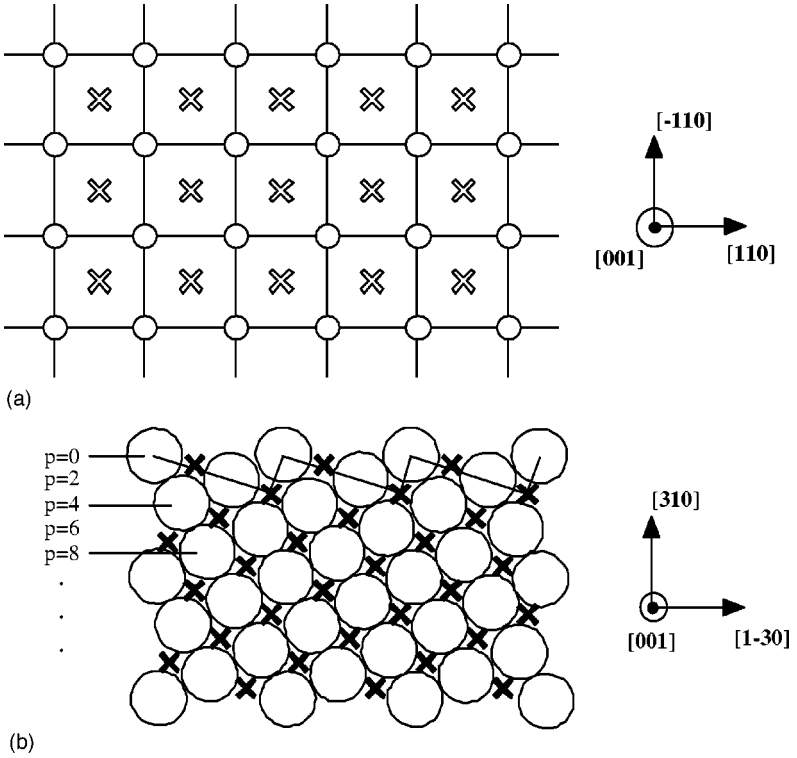

FIG. 1. (a) Top view of the structure of the (001) surface (a): the two symbols (circle and cross) correspond to the stacking of the two (002) planes along the [001] direction. (b) Side view of the structure of the (310) surface: the surface plane (label 0) and the underlayers ($p = 1,2,\ldots$) are indicated. The sites belonging to the odd planes (indicated by the crosses) are shifted by $a/2$ [001] relative to the ones belonging to the even planes (indicated by the circles).

obtained using the quasiharmonic approximation[51] and eight levels in the recursion method, lead to a vibrational contribution that can be neglected at the surface but which is significant for some GB sites.[41] Thus the SMA-TBIM approach yields a lattice-gas model with energetic and vibrational entropic parameters consistent with *N*-body interatomic potentials, and incorporates the influence of atomic relaxations.

III. SURFACE AND GB SEGREGATION DRIVING FORCES

The geometry and the numbering of the various sites of the interfaces studied in the present work are shown in Fig. 1 for the surfaces, and in Fig. 2 for the GB. The (310) surface can be also considered as a vicinal surface with (001) terraces and periodic steps along the $\langle 001 \rangle$ direction [see Fig. 1(b)]. The GB structure shown in Fig. 2, referred to as the *C* structure in previous works,[52] is characterized by a stacking of two different (002) planes along the tilt axis. Moreover, due to the collapse of two (620) planes into one during relaxation,[52] the boundary plane contains twice as many atoms as any other layer. However, these atomic sites are nonequivalent, the 0 sites being characterized by a large tensile pressure;[42] see Fig. 2. We must then distinguish two sublattices in this plane, which we denote c_0 and $c_{0'}$, for the Ag concentration on the respective sublattices in the GB plane.

As shown in Sec. II, the calculation of the segregation isotherm in the SMA-TBIM approach requires a knowledge of $\Delta H_p^{impurity}$ and the EPI's in the bulk and near the interface. $\Delta H_p^{impurity}$ is the enthalpy difference occurring when one substitutes a solute atom from a bulk site for a solvent atom at a site of the pth plane parallel to the interface; the relaxation procedure mentioned above being used in both the

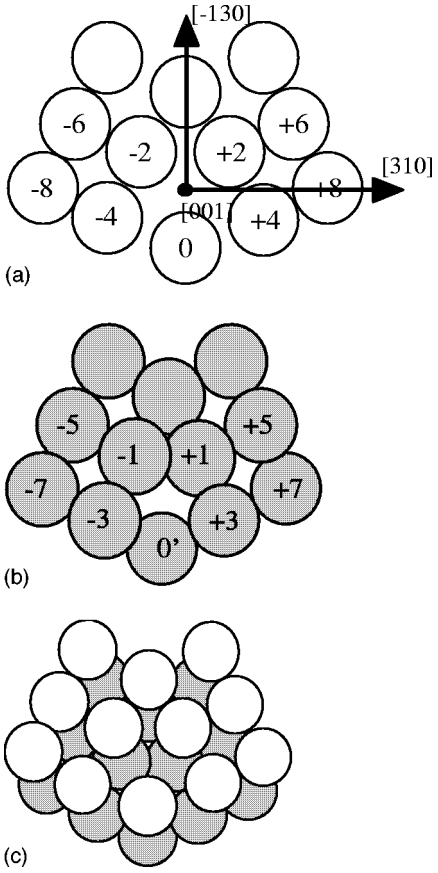

FIG. 2. Structure of the $\Sigma = 5$ (310) [001] tilt grain boundary. The sites $0, \pm 2, \pm 4, \ldots$ belong to the first (002) plane (a), whereas the sites $0', \pm 1, \pm 3, \ldots$ belong to the second (002) plane (b). A superimposition of these two planes along the tilt axis [001] is shown in (c).

TABLE I. Site enthalpy excess ΔH_p^{site}, size effect ΔH_p^{size}, EPI effect ΔH_p^{EPI}, and comparison between the segregation enthalpy of one impurity, $\Delta H_p^{impurity}$, and its estimation, $\Delta \tilde{H}_p^{impurity}$, from the sum of the three previous effects for the first three planes of the (001) surface. All these quantities are expressed in meV/at.

	ΔH_p^{site}	ΔH_p^{size}	ΔH_p^{EPI}	$\Delta \tilde{H}_p^{impurity}$	$\Delta H_p^{impurity}$
$p=0$	−130	−305	−109	−544	−541
$p=1$	−13	+8	−16	−21	−1
$p=2$	0	−3	0	−3	+4

initial and final states.[42] The three contributions ΔH_p^{site}, ΔH_p^{size}, and ΔH_p^{EPI} to $\Delta H_p^{impurity}$ are given in Tables I–III for the three interfaces and their sum, denoted $\Delta \tilde{H}_p^{impurity}$, is compared to the direct evaluation of $\Delta H_p^{impurity}$.

We note that $\Delta \tilde{H}_p^{impurity}$ reproduces $\Delta H_p^{impurity}$ very well in all cases, the maximum deviation being less than 60 meV. This shows the pertinence of the lattice-gas approach and the validity of the decomposition of the segregation enthalpy following Eq. (4). Moreover, it allows one to compare the segregation driving forces for the different interfaces.

(a) For the (001) surface, the segregation enthalpy for one isolated solute atom is significant only on the surface plane and almost vanishes for the first underlayer (see Table I). The size effect favors Ag segregation, due to the larger atomic radius of Ag compared to Cu ($r^{Ag}/r^{Cu}=1.13$).[3] The sign of the term ΔH_0^{site}, which is related to the lower surface energy of Ag compared to Cu, is also in favor of Ag segregation.[3] Finally, as Cu-Ag is a system that has a tendency to phase separate, the EPI effect favors the superficial enrichment of the minority element,[3] here Ag in the Cu(Ag) solid solution. Thus, for this surface, each of the three effects leads to Ag segregation, the size effect being the dominant contribution.

(b) For the more open (310) surface, the segregation enthalpy is greater than 100 meV (in absolute value) up to the fourth layer (see Table II); this corresponds strictly to the nearest-neighbor range. The size effect is again the dominant one, the relative influence of the site and EPI effects being very similar to the one observed for the (001) surface. If the (310) surface is considered as a vicinal surface with (001) terraces, then site 1, which is in the center of the (001) terrace, must have properties similar to the 0 site of the (001) surface. The comparison of the segregation enthalpy for both sites (see Tables I and II) shows that this is the case.

TABLE II. Site enthalpy excess ΔH_p^{site}, size effect ΔH_p^{size}, EPI effect ΔH_p^{EPI}, and comparison between the segregation enthalpy of one impurity, $\Delta H_p^{impurity}$, and its estimation, $\Delta \tilde{H}_p^{impurity}$, from the sum of the three previous effects for the first seven planes of the (310) surface. All these quantities are expressed in meV/at.

	ΔH_p^{site}	ΔH_p^{size}	ΔH_p^{EPI}	$\Delta \tilde{H}_p^{impurity}$	$\Delta H_p^{impurity}$
$p=0$	−213	−317	−172	−702	−659
$p=1$	−139	−288	−125	−552	−532
$p=2$	−98	−282	−85	−465	−457
$p=3$	−41	−83	−40	−164	−157
$p=4$	−12	+40	−16	+12	−31
$p=5$	−12	+4	−16	−24	0
$p=6$	−1	−12	0	−13	−2

TABLE III. Site enthalpy excess ΔH_p^{site}, size effect ΔH_p^{size}, EPI effect ΔH_p^{EPI}, and comparison between the segregation enthalpy of one impurity, $\Delta H_p^{impurity}$, and its estimation, $\Delta \tilde{H}_p^{impurity}$, from the sum of the three previous effects for the first five (620) adjacent planes of the $\Sigma=5$ (310) [001] tilt grain boundary and for the GB plane (sites 0 and 0'). All these quantities are expressed in meV/at.

	ΔH_p^{site}	ΔH_p^{size}	ΔH_p^{EPI}	$\Delta \tilde{H}_p^{impurity}$	$\Delta H_p^{impurity}$
$p=0$	+57	−578	+14	−507	−565
$p=0'$	−62	−91	−46	−199	−138
$p=\pm1$	−52	−69	−14	−135	−119
$p=\pm2$	−11	−191	−9	−211	−204
$p=\pm3$	−16	−116	0	−132	−131
$p=\pm4$	−15	−87	−16	−118	−99
$p=\pm5$	−4	+40	0	+36	+32

(c) For the $\Sigma=5$ (310) [001] GB, the segregation enthalpy is significant (i.e., greater than 100 meV in absolute value) on the GB plane (sublattices 0 and 0′) and on four (620) planes immediately adjacent to the interface (see Table III). This means that the spatial range of the segregation enthalpy on each side of the interface is one plane greater than for the (310) surface. As discussed previously,[27,42] GB segregation is largely dominated in the infinitely dilute limit by the size effect, due to the large distortions of the interatomic distances in the GB region. Nevertheless, the site effect cannot be neglected on sites 0′ and ±1, whereas the EPI effect remains almost negligible at all sites. An important contribution of the vibrational entropy to the Gibbs free energy of segregation on site 0 was found in a previous work, and must be taken into account in Eq. (1); see Table IV.[41]

Beyond the infinitely dilute limit the dependence of the segregation enthalpy on the local concentrations is given by the EPI's, which can differ near the interface from their bulk values.[3,44–46] In Table V we note that the EPI's within the (001) surface plane, $V_1^{0,0}$ and $V_2^{0,0}$, are less negative than in the bulk, indicating a lower tendency toward phase separation at the surface. A similar evolution was found by Meunier *et al.*,[46] using a slightly different interatomic potential for the Cu-Ag system. Conversely, the in-plane EPI's are enhanced (in absolute value) in the first underlayer, just as the inter-

TABLE IV. Vibrational part of the segregation entropy for the 0 sites of the $\Sigma=5$ (310) [001] tilt grain boundary, ΔS_0^{seg} (expressed in units of k_B) vs T and the contribution $-T\Delta S_0^{seg}$ (in meV/at.) to the Gibbs free energy of segregation, ΔG_0^{seg}.

T	300 K	600 K	900 K
ΔS_0^{seg}	−2.15	−2.5	−3.2
$-T\Delta S_0^{seg}$	+55	+130	+250

TABLE V. Number of neighbors $Z_R^{p,p+p'}$ and effective pair interactions between sites of planes p and $p+p'$, $V_R^{p,p+p'}$ (in meV), for the (001) surface. The numbers on the left (respectively on the right) are relative to the nearest neighbors: $R=1$ (respectively next-nearest neighbors: $R=2$).

	$p'=0$	$p'=1$	$p'=2$
$Z_R^{p,p+p'}$	4,4	4,0	0,1
$p=0$	$-18,-7$	$-51,-$	$-,-8$
$p=1$	$-31,-19$	$-30,-$	$-,-16$
$p=2$	$-25,-18$	$-24,-$	$-,-16$
bulk	$-23,-16$	$-23,-$	$-,-16$

layer EPI's $V_1^{0,1}$ and $V_1^{1,2}$. We note that the EPI's almost reach their bulk values beginning with the second underlayer.

The (310) surface has no nearest neighbors within the surface plane ($Z_1^{p,p}=0$; see Table VI). We show in Sec. IV this has an important consequence on the segregation isotherm. Similar to the (001) orientation, the in-plane EPI's $V_2^{p,p}$ are less negative than in the bulk for the first three planes ($0\leqslant p\leqslant 2$) (see Table VI), whereas some interlayer EPI's are strongly enhanced in absolute value. Moreover, if we analyze the results of the (310) surface as those for a vicinal orientation of the (001) surface, we find good agreement between the different values of the EPI's for the vicinal surface and for the flat one (see Table VII). We note that the EPI's reach almost their bulk values from the plane $p=5$ for

TABLE VI. Number of neighbors $Z_R^{p,p+p'}$ and effective pair interactions between sites of planes p and $p+p'$, $V_R^{p,p+p'}$ (in meV), for the (310) surface. The numbers on the left (respectively on the right) are relative to the nearest neighbors: $R=1$ (respectively next-nearest neighbors: $R=2$).

	$p'=0$	$p'=1$	$p'=2$	$p'=3$	$p'=4$	$p'=5$	$p'=6$
$Z_R^{p,p+p'}$	0,2	2,0	1,1	2,0	1,0	0,0	0,1
$p=0$	$-,-7$	$-29,-$	$-25,12$	$-50,0$	$-60,0$	$-,-$	$-,-12$
$p=1$	$-,-6$	$-13,-$	$-51,-16$	$-54,-$	$-55,-$	$-,-$	$-,-13$
$p=2$	$-,-12$	$-28,-$	$-47,-3$	$-53,-$	$-50,-$	$-,-$	$-,-13$
$p=3$	$-,-23$	$-44,-$	$-34,-16$	$-42,-$	$-48,-$	$-,-$	$-,-13$
$p=4$	$-,-22$	$-31,-$	$-29,-30$	$-29,-$	$-30,-$	$-,-$	$-,-18$
$p=5$	$-,-21$	$-27,-$	$-29,-19$	$-30,-$	$-29,-$	$-,-$	$-,-18$
bulk	$-,-16$	$-23,-$	$-23,-16$	$-23,-$	$-23,-$	$-,-$	$-,-16$

TABLE VII. Comparison between the effective pair interactions (in meV) of the (001) surface and the (310) surface considered as a vicinal surface of the (001) one.

(001)	$V_2^{0,0}=-7$	$V_1^{0,1}=-51$	$V_2^{0,2}=-8$	$V_1^{1,1}=-31$	$V_2^{1,1}=-19$	$V_1^{1,2}=-30$	$V_2^{1,3}=-16$
(310)	$V_2^{0,0}=-7$ $V_2^{1,1}=-6$	$V_1^{1,3}=-51$ $V_1^{1,4}=-54$ $V_1^{1,5}=-55$	$V_2^{0,6}=-12$ $V_2^{1,7}=-13$ $V_2^{2,8}=-13$	$V_1^{4,3}=-31$	$V_2^{4,4}=-22$	$V_1^{4,6}=-29$ $V_1^{4,7}=-29$ $V_1^{4,8}=-30$	$V_2^{4,10}=-18$

TABLE VIII. Effective pair interactions between sites of planes p and q, $V_R^{p,q}$ (in meV), for the (310) GB. The numbers on the left (respectively on the right) are relative to the nearest neighbors: $R=1$ (respectively next-nearest neighbors: $R=2$). For $V_2^{\pm 2,\pm 2}$, the two values correspond to different types of neighbors between the planes ± 2: $V_2^{+2,-2}$ on the left and $V_2^{\pm 2,\pm 2}$ on the right.

	$q=0$	$q=0'$	$q=\pm 1$	$q=\pm 2$	$q=\pm 3$	$q=\pm 4$
$p=0$	$-,-5$	$-6,-$	$-9,-$	$-44,-20$	$-29,-$	$-29,-$
$p=0'$		$-,-30$	$-44,-17$	$-1,-$	$6,-$	$-,-$
$p=\pm 1$			$30,-33$	$-29,-20$	$-20,0$	$-30,-$
$p=\pm 2$				$-,-2/-33$	$-33,-$	$-48,-19$
$p=\pm 3$					$-,-33$	$-28,-$
$p=\pm 4$						$-,-20$

TABLE IX. Number of neighbors between sites of planes p and q, $Z_R^{p,q}$, for the (310) GB. The numbers on the left (respectively on the right) are relative to the nearest neighbors: $R=1$ (respectively next-nearest neighbors: $R=2$). For $Z_2^{\pm 2,\pm 2}$, the two values correspond to different types of neighbors between the planes ± 2 (see Table VIII).

	$q=0$	$q=0'$	$q=\pm 1$	$q=\pm 2$	$q=\pm 3$	$q=\pm 4$
$p=0$	$-,-2$	$2,-$	$4,-$	$2,2$	$4,-$	$2,-$
$p=0'$		$-,2$	$2,2$	$4,-$	$2,-$	$-,-$
$p=\pm 1$			$1,2$	$2,2$	$1,2$	$2,-$
$p=\pm 2$				$-,2/1$	$2,-$	$1,1$
$p=\pm 3$					$-,2$	$2,-$
$p=\pm 4$						$-,2$

the (310) surface, which corresponds to the $p=2$ plane for the (001) orientation.

For the $\Sigma=5$ (310) [001] tilt GB, the EPI's and the coordination numbers between the sites in the first planes adjacent to the interface are given in Tables VIII and IX. The convergence of the EPI's toward their bulk values is rather similar to the (310) surface. However, the values in the GB plane (sites 0 and $0'$) and in the closest (620) planes parallel to the interface (sites ± 1) differ strongly from the ones obtained for the (310) surface. In particular, the maximum absolute value of the ratio $V_1^{p,q}/V_1^{bulk}$ is less: 2.1 instead of 2.6. Furthermore, a high positive value is obtained for $V_1^{-1,1}$ ($+30$ meV), indicating a repulsion between Ag solute atoms located in nearest-neighbor positions on planes -1 and $+1$. This repulsion is related to the strong compressive pressure on these sites;[42] see Fig. 2.

TABLE X. Solubility limit c_a and spinodal limit c_{spi}, calculated from mean-field equations for various temperatures.

T	300 K	600 K	900 K
c_α	5.0×10^{-7}	7.1×10^{-4}	8.5×10^{-3}
c_{spi}	3.6×10^{-2}	7.6×10^{-2}	12×10^{-2}

Using the energetic quantities ($\Delta H_p^{impurity}$ and the EPI's) described in this section, and assuming they do not depend on temperature and concentrations, in Sec. IV we show the segregation isotherms for the three interfaces, mainly studied at three temperatures (900, 600, and 300 K).

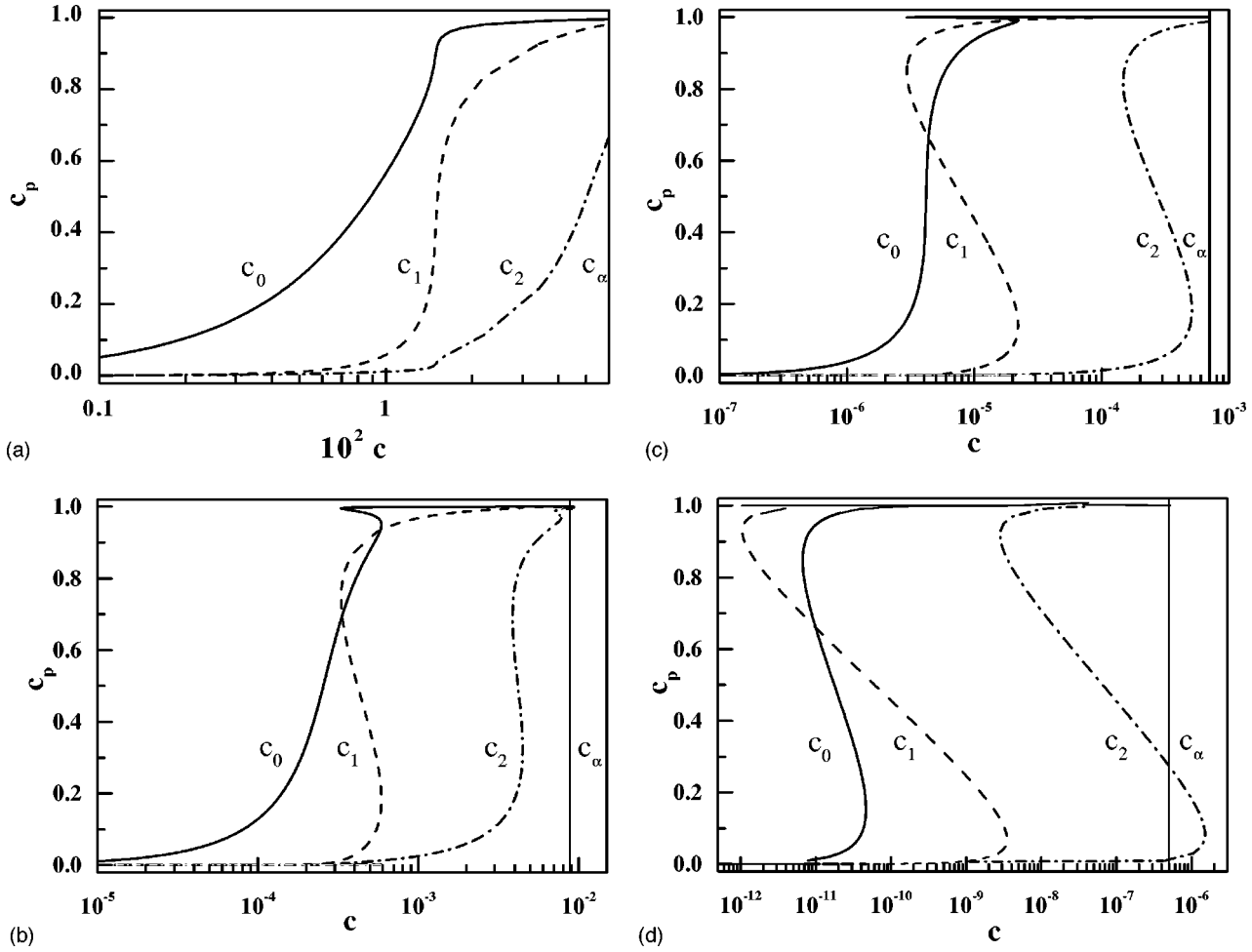

FIG. 3. Segregation isotherms for the (001) surface: c_p vs c for $p\leqslant 2$, at $T=1600$ K (a), 900 K (b), 600 K (c), and 300 K (d). The bulk solubility limit is indicated by the vertical line.

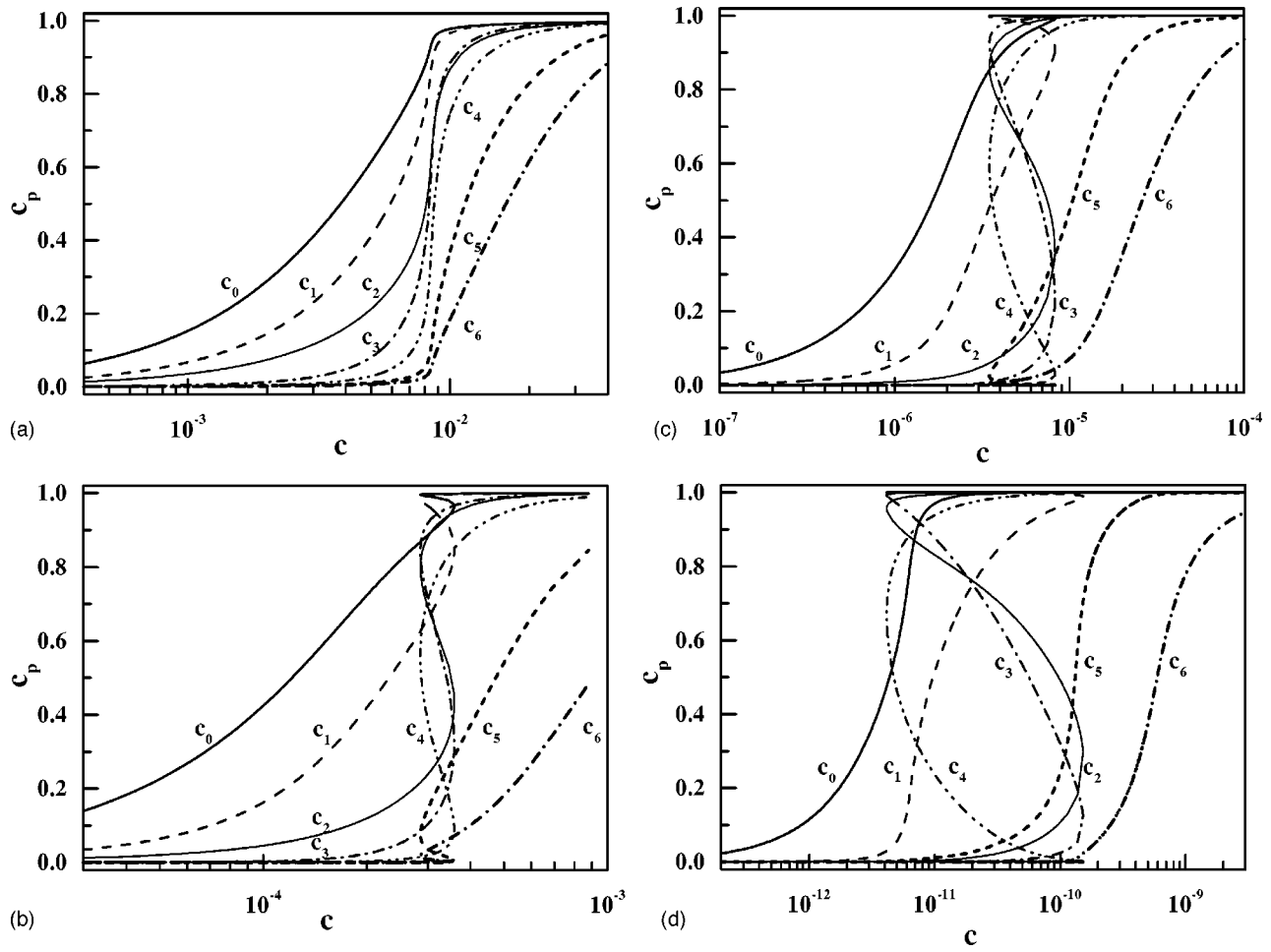

FIG. 4. Segregation isotherms for the (310) surface: c_p vs c for $p \leqslant 6$, at $T=1500$ K (a), 900 K (b), 600 K (c), and 300 K (d).

IV. SEGREGATION ISOTHERMS

The segregation isotherms are obtained by solving the system of nonlinear equations (1), coupled by means of the interaction term $\Delta H_p^{interaction}(c,c_p,c_{p'})$. This is performed by using a Newton-Raphson algorithm with a sufficiently large number of equations like Eqs. (1) for a given temperature.[34] Note that the study is restricted to the domain of the bulk solid-solution Cu(Ag), i.e. the Ag bulk concentration remains smaller than the solubility limit c_α, which is given by the following equation (see Table X):

$$\frac{c_\alpha(T)}{1-c_\alpha(T)} = \exp\left[\frac{(1-2c_\alpha(T))\sum_R Z_R V_R}{k_B T}\right]. \qquad (6a)$$

When the solubility limit is very low, as in the present case, this expression can be approximated by

$$c_\alpha(T) = \exp\left[\frac{\sum_R Z_R V_R}{k_B T}\right]. \qquad (6b)$$

A. (001) surface

In Fig. 3(a), the segregation isotherms are shown at $T=1600$ K, giving the concentration of the first three planes, from c_0 to c_2, as a function of the bulk concentration c. At this temperature, all the concentrations increase monotonously with c up to a value almost equal to 1 for c_0 and c_1 when c reaches the bulk solubility limit. $\Delta H_0^{impurity}$ being greater (in absolute value) than $\Delta H_1^{impurity}$ (see Table I), c_0 is greater than c_1 whatever c. At $T=900$ K [see Fig. 3(b)], c_0 increases almost monotonocally, whereas the c_1 curve is a van der Waals loop, indicating a first-order layering transition on this plane.[34] This transition is responsible for the small ''companion'' transition[35,53] observed in the upper part of the c_0 isotherm. For a higher bulk concentration, another first-order phase transition affects c_2 just before the bulk solubility limit c_α.

When decreasing the temperature, the isotherms on the different planes are shifted toward lower bulk concentrations. The surface critical temperature T_c^0, below which a first-order phase transition is observed on the surface plane, must be slightly less than 600 K in view of the c_0 curve in Figs. 3(c) and 3(d). The same consideration for the c_1 curve leads to an estimation of T_c^1 around 1500 K [see Fig. 3(a)]. In Sec. V we discuss the origin of such variations of the critical

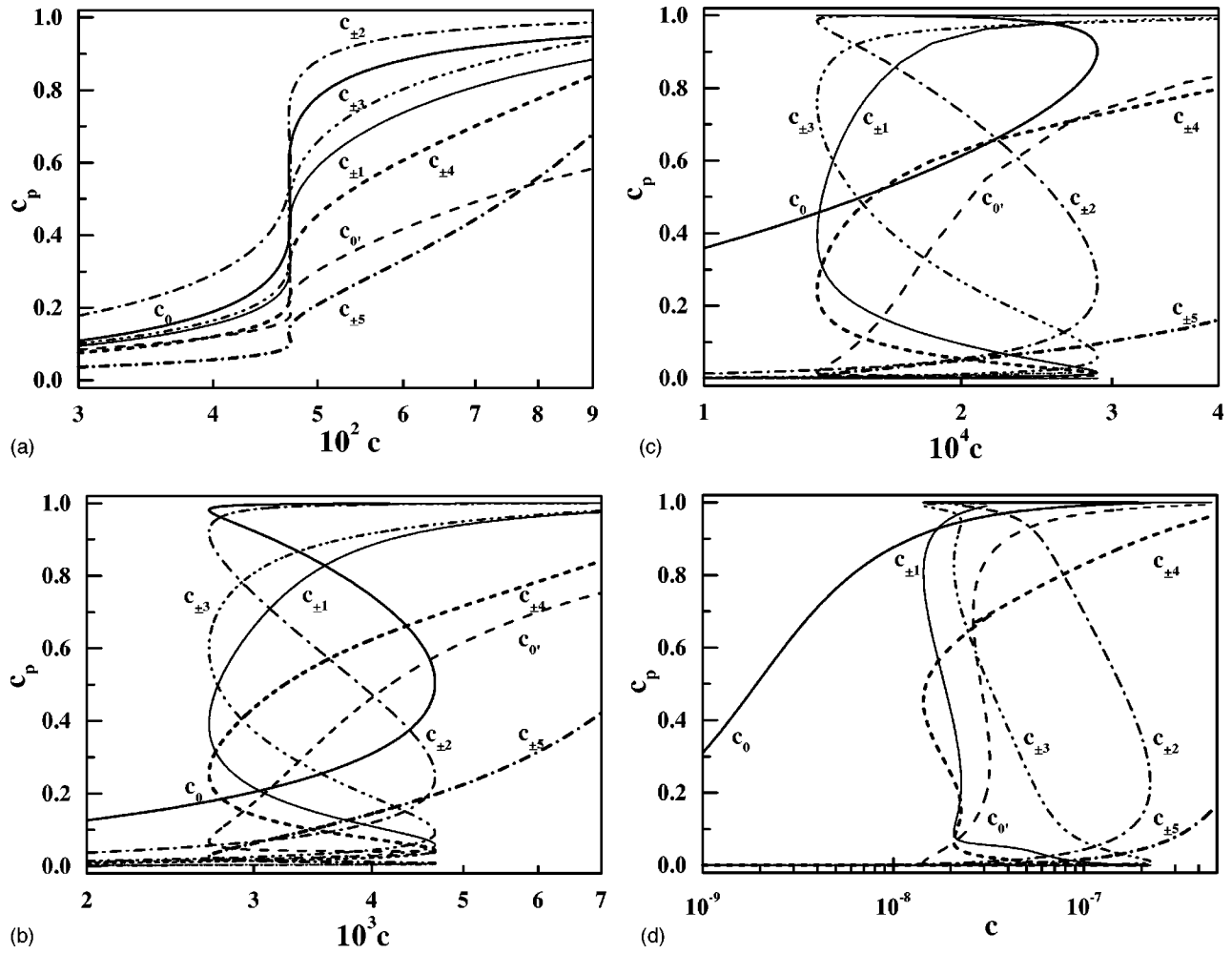

FIG. 5. Segregation isotherms for the $\Sigma=5$ (310) [001] tilt grain boundary: c_p vs c, for the grain boundary plane ($p=0$ and $0'$) and for the first adjacent planes $p\leqslant 5$, at $T=1600$ K (a), 900 K (b), 600 K (c), and 300 K (d). Note that the value of the vibrational segregation entropy at $T=1600$ K is taken equal to its value at 900 K. This leads to underestimate its effect on c_0.

temperature for the first-layer transitions. We note that the width of the van der Waals loops is larger (on a logarithmic scale) when the temperature decreases. As a consequence, the lower part of the c_2 isotherm goes beyond the bulk solubility limit at $T=300$ K without reaching the spinodal limit c_{spi}, given by (see Table X)

$$k_B T = -2c_{spi}(1-c_{spi})\sum_R Z_R V_R . \qquad (7)$$

However, this remark concerns only the metastable part of the isotherms, with the phase transition on these planes occurring before c_α.

Note that only the first layering transition has been identified clearly from an experimental point of view.[31] Other studies for the (111) face in Cu(Ag) alloys[34,54] lead to similar results, indicating kindred behaviors for these two close-packed surfaces. We discuss the properties of these isotherms in Secs. V and VI to explain their main characteristics, i.e., the existence of successive first-order phase transitions on different planes near the surface and the lower value of the critical temperature on the surface relative to the first underlayer plane.

B. (310) surface

The segregation isotherms for this open surface are shown in Figs. 4(a)–4(d) for $T=1500$, 900, 600, and 300 K. The main characteristic of these isotherms is the presence of a *multilayer* phase transition of first order affecting planes 2, 3, and 4. It differs strongly from the (001) surface, for which *successive monolayer* phase transitions are observed on planes 0, 1, and 2. A numerical estimation of the critical temperature $T_c^{(310)}$, above which the isotherms are monotonic, can be obtained from Fig. 4(a). At $T=1500$ K, all the isotherms are distinct and monotonic. However, the slope of the curves $c_p(c)$ is almost infinite near $c_p=0.5$ for $2\leqslant p \leqslant 4$, indicating that $T_c^{(310)}$ is slightly below 1500 K. Below $T_c^{(310)}$ the discontinuous increase of (c_2,c_3,c_4) at c_{trans} is preceded at lower bulk concentrations by a continuous increase of c_0 and c_1. At c_{trans} these two concentrations undergo a small companion transition in the upper part of the

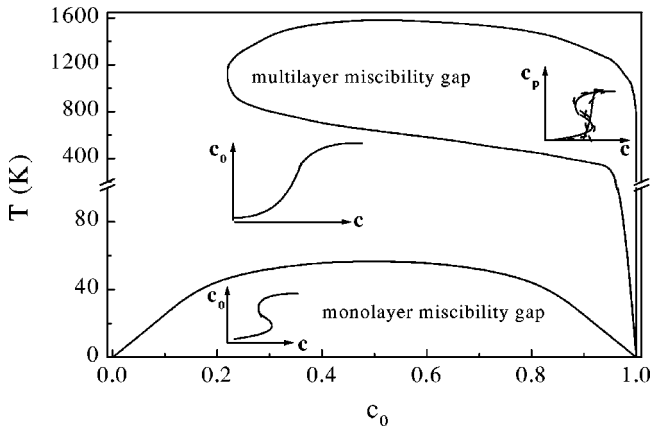

FIG. 6. Two-dimensional phase diagram for the 0 sites of the GB plane. This phase diagram includes a classical 2D symmetrical miscibility gap with $T_c = 58$ K and an asymmetrical miscibility gap with $T_c = 1600$ K due to the multilayer phase transition.

isotherms, very similar to the one observed for c_0 at $T = 900$ K for the (001) surface.

Let us compare the relative positions of the isotherms between the (001) and (310) surfaces. $c_1^{(310)}$ is very similar to $c_0^{(001)}$, consistent with the already mentioned analysis of the (310) surface as a vicinal surface with (001) terraces. The same analysis leads to a comparison of $c_4^{(310)}$ with $c_1^{(001)}$. The positions of these isotherms on the bulk concentration scale are similar. Moreover, as can be predicted from the segregation enthalpy in the infinitely dilute limit (see Tables I and II), the $c_0^{(310)}$ curve is shifted toward a lower bulk concentration when compared to the $c_0^{(001)}$ curve. This arises from the larger number of missing bonds for the atom 0 on the (310) surface, which can be considered as a step edge atom of this vicinal surface.

In Sec. V we analyze the origin of the multilayer phase transition observed for this open surface, which differs from the succession of monolayer phase transitions obtained for the (001) surface.

C. $\Sigma = 5$ (310) [001] GB

The segregation isotherms for this symmetrical tilt grain boundary are shown in Figs. 5(a)–5(d) for $T = 1600$, 900, 600, and 300 K. Note that we impose a symmetrical concentration profile by assuming $c_{-p} = c_p$. Similar to the (310) surface, the main characteristic of these isotherms is the presence of a *multilayer* phase transition affecting the first four adjacent planes, p, on each side of the GB plane: $p = \pm 1$ to ± 4.

Concerning the GB plane itself, the situation is intricate. For the 0 sites, the influence of the temperature leads to a remarkable phenomenon. Actually, the vibrational segregation entropy, which can be neglected at the surface,[47] significantly reduces the Gibbs free energy of segregation on the site 0 in the GB plane when T increases (see Table IV). This is at the origin of the strong evolution of the segregation isotherm for the 0 sites with temperature. At 900 and 600 K, the 0 sites clearly contribute to the multilayer phase transition as revealed by the large jump of c_0 at $c_{trans}(T)$; see Figs. 5(b) and 5(c). Conversely, at lower temperature [$T = 300$ K; see Fig. 5(d)], the isotherm of the 0 sites is shifted strongly toward a lower bulk concentration relative to c_{trans}

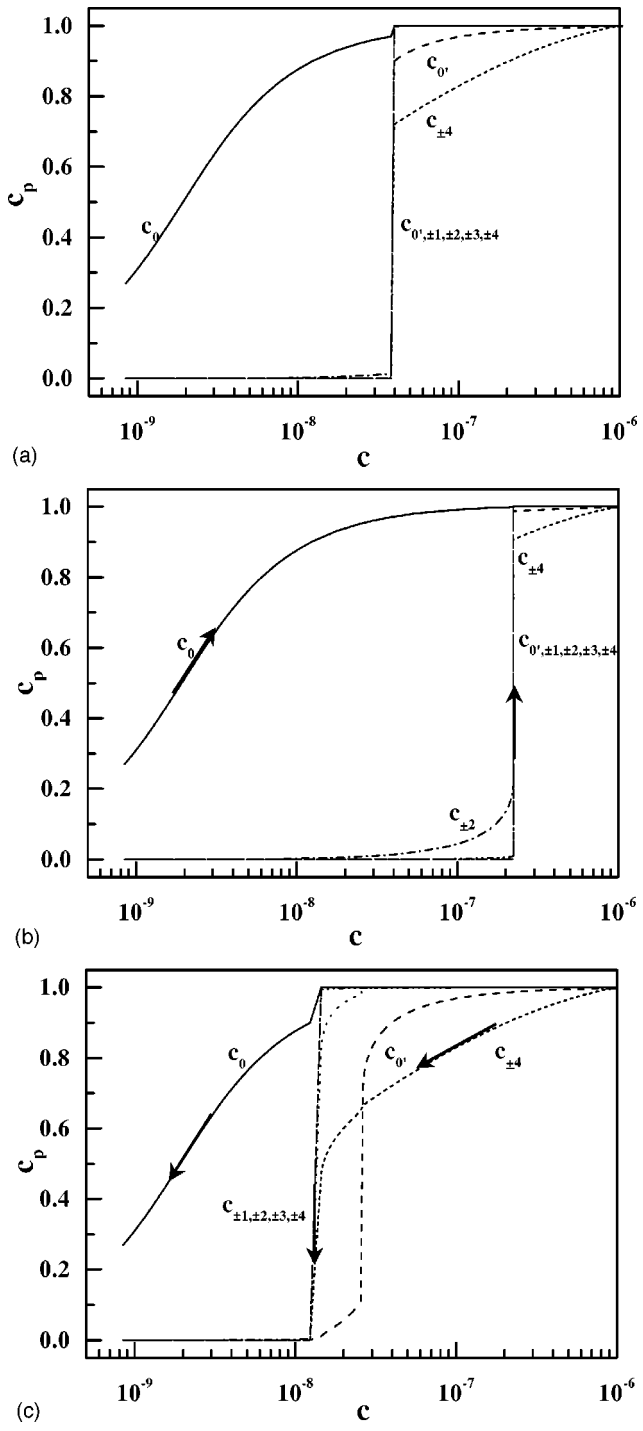

FIG. 7. Segregation isotherms for the main planes of the $\Sigma = 5$ (310) [001] tilt grain boundary, c_p vs c, at $T = 300$ K. Only the most stable states are shown in (a), whereas the hysteresis cycle is indicated in (b) and (c). The isotherms obtained by increasing c are shown in (b), and correspond to only one multilayer phase transition, whereas the isotherms obtained by decreasing c, shown in (c), present two phase transitions.

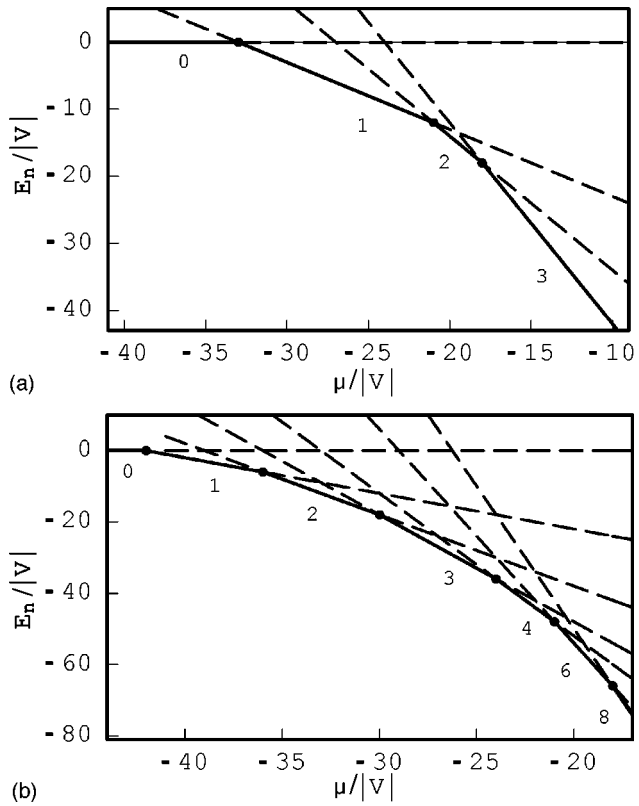

FIG. 8. The normalized ground-state internal energies $E_n/|V|$ vs the difference in normalized chemical potentials $\mu/|V|$ within the broken-bond model [see Eqs. (8) and (9)], with $\Delta\tau/V=4$ for the (001) surface (a) and the (310) surface (b). Solid (broken) lines represent stable (metastable) states and the number of A layers in each state is marked in the figure.

(300 K), and becomes almost monotonic. Actually, this isotherm is no longer affected by the multilayer phase transition, except by the presence of a small companion transition of very weak amplitude near $c_0=1$. However, at very low temperature, the isotherm for the 0 sites recovers the same behavior as the one observed for the (001) surface: for $T<T_c^0\approx 60$ K, there is a monolayer phase transition affecting this isotherm. *Thus the two-dimensional* $(2D)$ *phase diagram for the* 0 *sites, obtained by drawing the* $2D$ *solubility limit as a function of T, presents a multireentrant phase transition shown in Fig. 6.* This arises from the existence of a first miscibility gap due to the monolayer phase transition for $T<60$ K and a second miscibility gap issued from the multilayer phase transition for $T<1600$ K.

If we examine closely the GB phase transition at $T=300$ K [Fig. 5(d)], we note that the multilayer phase transition occurring at higher temperature splits up into three phase transitions. The first transition affects mainly $c_{\pm 2}$ and $c_{\pm 3}$. When these concentrations are located in the high part of the isotherm, a second transition affects $c_{\pm 1}$ and $c_{\pm 4}$ (near $c=2.2\times 10^{-8}$) followed by a third one affecting $c_{0'}$ (near $c=3\times 10^{-8}$). However, if we consider only the most stable state for each bulk concentration, there is a unique transition at $c=3.810^{-8}$, affecting the GB plane (sites $0'$) and the first four adjacent planes on each side of the GB plane [see Fig. 7(a)]. Conversely, the metastable states are important when studying the kinetics of segregation or depletion.[55,56] The complexity of the equilibrium isotherms at $T=300$ K must lead to an unexpected kinetic behavior. More precisely, the hysteresis cycle, which can be derived from these kinetics using the local equilibrium concept,[56,57] has the peculiarity to present one transition when c increases [kinetics of segregation, see Fig. 7(b)] and two transitions when c decreases [kinetics of depletion, see Fig. 7(c)].

Similar to the case of the (310) surface, we numerically determine the critical temperature of the GB multilayer phase transition. Figure 5(a) shows that T_c^{GB} is about 1600 K and is slightly higher than $T_c^{(310)}=1500$ K, whereas the critical bulk concentration c_{trans} is much higher for the GB than for the (310) surface at all temperatures (compare Figs. 4 and 5). This last point is related to the higher absolute value of the segregation enthalpies for the (310) surface, at least for the first three planes (see Tables II and III).

V. SIMPLE ANALYTICAL MODELS

In this section we attempt to elucidate the main factors at the origin of the differences observed between the isotherms for the (001) and (310) surfaces and the $\Sigma=5$ (310) [001] GB. For the (001) surface, layering transitions affecting successively the first surface planes are obtained, whereas a multilayer phase transition is found for the other two interfaces. We first present a ground-state analysis at $T=0$ K. This allows us to discriminate the influence of the various energetic quantities and the crystallographic parameters on the monolayer-multilayer character of the interfacial phase transition.[56,58] Then we present a very simple bilayer model to show how the critical temperature is affected by the multilayer nature of the phase transition. A more detailed comparison of these simple analytical models with the numerical results obtained in the previous section is presented in Sec. VI.

A. Ground-state properties of interfacial segregation

To give more insight into the domain of existence of the multilayer phase transition, we use a simple Hamiltonian, for which only the EPI's between nearest and next-nearest neighbors are considered. Moreover, in view of the small difference between V_1 and V_2 (see Tables V–VIII) and in order to reduce the number of parameters, the EPI's are all assumed to have the same value as in the bulk : $V_1^{p,q}=V_2^{p,q}=V$, $\forall$ p, q. For the segregation enthalpy in the dilute limit, $\Delta H_p^{impurity}$, we adopt the expression derived from a simple broken-bond model,[3]

$$\Delta H_p^{impurity}=\sum_{q>2p} Z^{p,q}(\Delta\tau+V), \tag{8a}$$

where $Z^{p,q}$ denotes the coordination number including nearest and next-nearest neighbors, and

$$\Delta\tau=(V_{BB}-V_{AA})/2. \tag{8b}$$

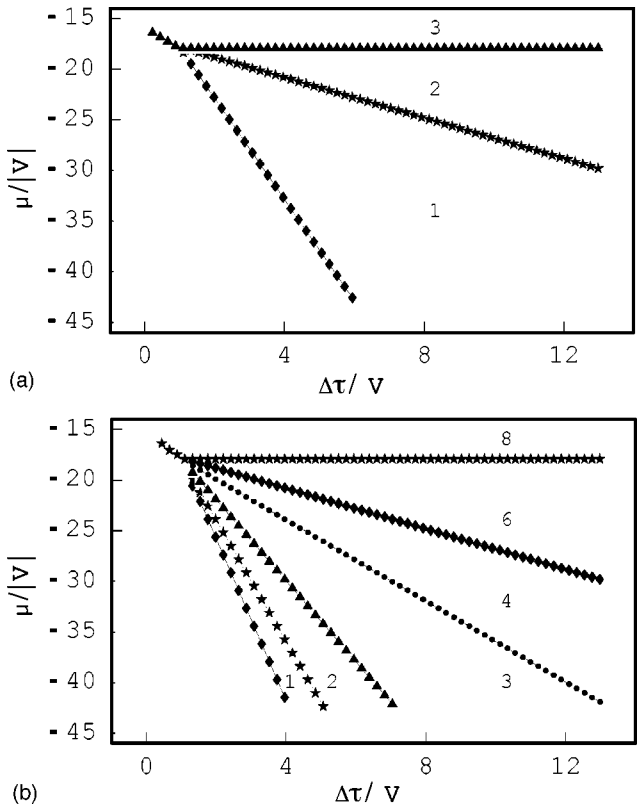

FIG. 9. The global ground-state phase diagram for the simple broken-bond model [see Eqs. (8) and (9)] for the (001) (a) and (310) surfaces (b). This represents the location of layering or multilayer transition (in $\mu/|V|$) as a function of the energetic parameter $\Delta\tau/V$. The numbers in the figure mark regions corresponding to states with different numbers of A layers.

This leads to a model with two energetic quantities V and $\Delta\tau$. In order to determine the relative influence of the energetic and crystallographic parameters on the occurrence of a multilayer transition, we consider the ground-state properties of the model for the (001) and (310) surfaces. Toward this goal, we compare the internal energies of systems with n A layers, E_n, for various values of n as a function of the difference in chemical potentials $\mu=\mu_A-\mu_B$. E_n is obtained as

$$E_0(\mu)=0, \tag{9a}$$

$$E_1(\mu)=\Delta H_0^{impurity}+Z^{0,0}V-\mu, \tag{9b}$$

$$E_n(\mu)=\sum_{p=0}^{n-1}\Delta H_p^{impurity}+\sum_{p=0}^{n-1}Z^{p,p}V + 2\sum_{p=0}^{n-1}\sum_{0\leqslant p-q\leqslant p-1}Z^{p,p-q}V-n\mu. \tag{9c}$$

Figure 8 shows the lines $E_n(\mu)/|V|$ for the two surfaces for a given value of $\Delta\tau/V$. We note that the main characteristics of the various isotherms (monolayer or multilayer phase transitions) are already present in the interfacial ground states. In particular, the (001) surface is characterized by a sequence of layering transitions: $0\rightarrow1$, $1\rightarrow2$, $2\rightarrow3$ [Fig. 8(a)], whereas a multilayer transition $4\rightarrow6$ is observed for the (310) surface [Fig. 8(b)]. This demonstrates that, for a given set of energetic parameters $(\Delta\tau,V)$, the change in intra-layer and interlayer coordination numbers between the (001) and the (310) surfaces is sufficient to explain the occurrence of a multilayer transition for the open surface.

In Fig. 9 we compare the global ground-state phase diagrams for the (001) and (310) surfaces, i.e., the normalized chemical potential $(\mu/|V|)$ at all possible transition points as a function of the parameter $\Delta\tau/V$. For $\Delta\tau/V>1$, which corresponds to the wetting regime in terms of multilayer adsorption,[59] the (001) surface is characterized by a succession of layering transitions [Fig. 9(a)], whereas the (310) surface presents a multilayer transition: $4\rightarrow6$ [Fig. 9(b)]. This indicates that the distinction between layering transitions for relative close-packed surfaces as the (001) surface and multilayer transitions for open surfaces as the (310) surface does not depend on the energetic quantities $(\Delta\tau,\ V)$ in this very simple model, but is due only to the crystallographic parameters. Remember, however, that the multilayer phase transition $4\rightarrow6$, which is predicted for the (310) surface, differs from the $2\rightarrow5$ transition obtained for the same surface with the SMA-TBIM Hamiltonian [Eqs. (2)–(5)], see Sec. IV B. In Sec. VI A we discuss the origin of such discrepancy, and we show in particular the influence of the variation of the EPI's near the surface.

B. Critical temperature within the monolayer and the bilayer model

In this section, we analyze the respective role of the intralayer and interlayer couplings on the critical temperature. First of all, when the ground state clearly indicates a sequence of layering transitions $0\rightarrow1$, $1\rightarrow2$, $2\rightarrow3$, as for the (001) surface, we can estimate the critical temperature for the p-plane transition by considering that all the concentrations, except c_p, remain constant close to the transition.[34] This leads to the so-called monolayer model, and Eqs. (1)–(5) become

$$\frac{c_p}{1-c_p}=\frac{c}{1-c}\exp\left[-\frac{A_p+B_{pp}c_p}{k_BT}\right], \tag{10}$$

with

$$A_0=\Delta H_0^{impurity}, \tag{11a}$$

$$A_p=\Delta H_p^{impurity}+2\sum_R\sum_{p'=0}^{p-1}Z_R^{p',p}V_R^{p',p}, \quad p>0 \tag{11b}$$

$$B_{pp}=2\sum_R Z_R^{p,p}V_R^{p,p} \quad \text{for } p\geqslant0. \tag{11c}$$

Equations (10) and (11) have been obtained employing the following additional assumptions: (a) due to the low solubility, the bulk concentration remains always very small and has been neglected in front of A_p in the exponential argument; (b) without loss of generality, the constant values for c_q with

$q \neq p$ have been chosen as $c_q \approx 1$ for $q < p$ and $c_q \approx 0$ for $q > p$; and (c) the vibrational part of the segregation entropy has been neglected, as this is justified for the (001) surface.[47]

Equations (10) and (11) are simply the well-known Fowler-Guggenheim equation, which leads to the existence of a first-order phase transition on the pth plane.[25] Below a critical temperature T_c^p the pth plane isotherm presents a symmetrical van der Waals loop [see Figs. 3(b)–3(d)]. The critical bulk concentration c_{trans}^p, at which the transition occurs on the pth plane, is given by[34]

$$c_{trans}^p(T) = c(c_p = 0.5) = \exp\left[\frac{A_p + B_{pp}/2}{k_B T}\right], \tag{12}$$

which can be also expressed as a function of the solubility limit c_α [see Eq. 6(b)]:

$$c_{trans}^p(T) = c_\alpha \exp\left[\frac{A_p + B_{pp}/2 - \sum_R Z_R V_R}{k_B T}\right]. \tag{13}$$

Equation (13) gives the condition $A_p + B_{pp}/2 - \Sigma_R Z_R V_R < 0$, which must be fulfilled to obtain the transition for a bulk concentration inside the domain of the solid solution. The critical temperature for the pth plane transition corresponds to the one of a 2D system characterized by coordination numbers equal to $Z_R^{p,p}$, and EPI's equal to $V_R^{p,p}$ (Ref. 34):

$$T_c^p = -B_{pp}/4k_B = -\sum_R Z_R^{p,p} V_R^{p,p}/2k_B. \tag{14}$$

A succession of layering transitions is obtained in this monolayer model as long as the equilibrium equation (10) for the pth plane differs from the generic bulk one, either by the presence of the $\Delta H_p^{impurity}$ term or by a variation of the EPI's $V_R^{p,p'}$. To summarize the main characteristics of the monolayer model, note that the critical temperature depends only on the *intralayer* EPI's, $V_R^{p,p}$ and on the *intralayer* coordination numbers $Z_R^{p,p}$, whereas the position of the isotherms, characterized by c_{trans}^p, depends mainly on $\Delta H_p^{impurity}$ and on the *interlayer* EPI's and *interlayer* coordination numbers.

Let us now consider the case of the (310) surface, for which the ground-state analysis and the isotherms indicate the existence of a multilayer transition. An important crystallographic property of the (310) planes is its intralayer coordination number: there is no nearest neighbor and only two next-nearest neighbors within the plane, see Table VI. As the critical temperature depends only on the *intralayer* EPI's and coordination numbers within the simple monolayer model, very low values of T_c^p are expected from Eq. (14). Thus, using the values of the intralayer EPI's given in Table VI, the minimum value of T_c^p is equal to 70 K and is obtained for $p = 1$, whereas the maximum value is equal to 270 K for $p = 3$. All these values are much lower than the numerical estimation of the critical temperature for the multilayer phase transition given in Sec. IV B, which is about 1500 K; see Fig. 4(a). However, it is obvious that the main hypothesis of the monolayer model, which assumes that the concentrations c_q with $q \neq p$ remain constant near the transition affecting the pth plane, is unjustified for a multilayer phase transition.

To explain the large increase of the critical temperature relative to the prediction of the monolayer model, we present a simple bilayer model, which captures the essential features of the multilayer phase transition. Let us assume that the transition affects the planes p and $q = p + 1$. As an extension of the monolayer approach, we assume in the bilayer model that all concentrations, except c_p and c_{p+1}, remain constant near the phase transition. Moreover, we retain the additional hypothesis used in the monolayer model, in particular $c_{p'} = 1$ for $p' < p$ and $c_{p'} = 0$ for $p' > q$. This leads to the two nonlinear coupled equations

$$\frac{c_p}{1 - c_p} = \frac{c}{1 - c} \exp\left[-\frac{A_p + B_{pp} c_p + B_{pq} c_q}{k_B T}\right], \tag{15a}$$

$$\frac{c_q}{1 - c_q} = \frac{c}{1 - c} \exp\left[-\frac{A_q + B_{qp} c_p + B_{qq} c_q}{k_B T}\right], \tag{15b}$$

with

$$A_0 = \Delta H_0^{impurity}, \tag{16a}$$

$$A_p = \Delta H_p^{impurity} + 2 \sum_R \sum_{p'=0}^{p-1} Z_R^{p',p} V_R^{p',p} \quad \text{with} \quad p > 0, \tag{16b}$$

$$B_{pq} = B_{qp} = 2 \sum_R Z_R^{p,q} V_R^{p,q} \quad \text{with} \quad p \geqslant 0 \quad \text{and} \quad q \geqslant 0. \tag{16c}$$

The critical temperature is given by the equations.

$$\left(\frac{\partial c}{\partial c_p}\right)_{c_p^{crit}} = \left(\frac{\partial c}{\partial c_q}\right)_{c_q^{crit}} = 0 \quad \text{and}$$

$$\left(\frac{\partial^2 c}{\partial c_p^2}\right)_{c_p^{crit}} = \left(\frac{\partial^2 c}{\partial c_q^2}\right)_{c_q^{crit}} = 0. \tag{17}$$

An analytical expression of $T_c^{bilayer}$ can be obtained if we assume, in addition, that $c_p^{crit} = c_q^{crit} = 0.5$. It is easy to show that this corresponds to the upper limit of T_c, which is[47]

$$T_c^{bilayer} = -\frac{(B_{pp} + B_{qq}) - \sqrt{(B_{pp} - B_{qq})^2 + 4B_{pq}^2}}{8k_B}. \tag{18}$$

We recover the result of the monolayer model when $B_{pq} = 0$. In this case, Eq. (18) becomes

$$T_c^{monolayer} = \frac{Max(-B_{pp}, -B_{qq})}{4k_B}, \tag{19}$$

which is equivalent to Eq. (14).

The main value of Eq. (18) is to show that the *interlayer* coupling term B_{pq} *increases* the critical temperature relative to the value given by the monolayer model. This result is in

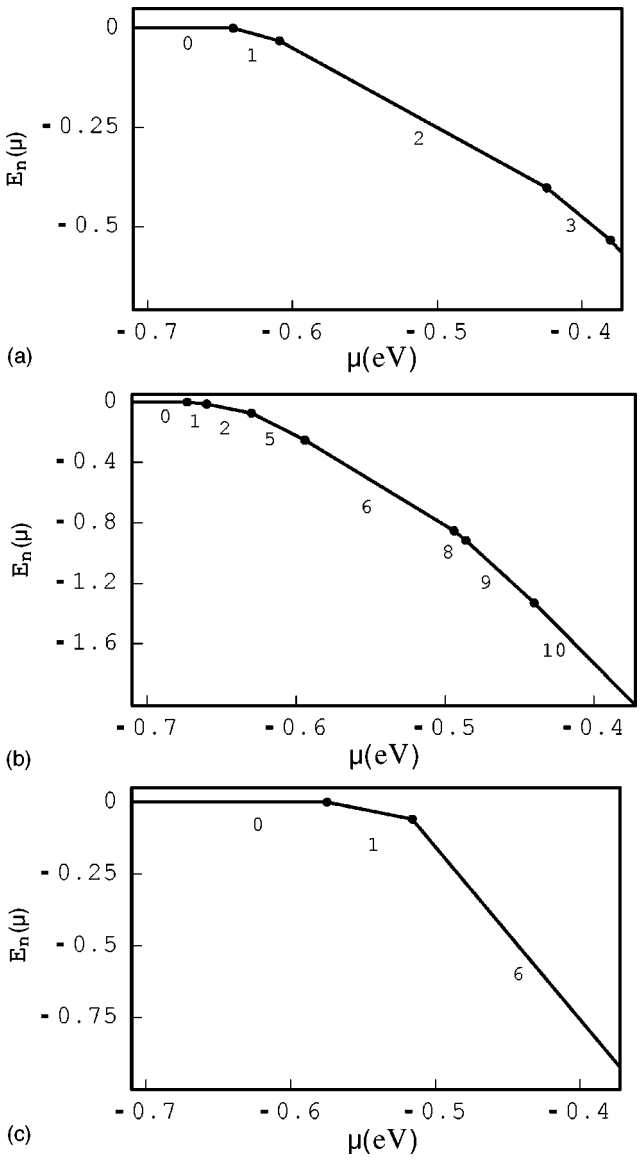

FIG. 10. The ground-state internal energies (in eV) vs the difference in chemical potentials (in eV) for the (001) surface (a), the (310) surface (b), and the (310) GB (c). Only the stable states are represented, and the number of Ag layers in each state is marked in the figure.

agreement with the relative values of the critical temperature for the multilayer phase transition for the (310) surface ($T=1500$ K) and the maximum critical temperature obtained within the monolayer model (270 K).

VI. DISCUSSION

If the simple analytical models presented above capture the main characteristics of the multilayer phase transition observed for the open interfaces [the (310) surface and the (310) [001] tilt GB], we can wonder how they compare with the results of Sec. IV obtained from the numerical resolution of Eqs. (1)–(5). In particular, is the ground-state analysis able to predict the precise sequence of monolayer-multilayer phase transitions for the three interfaces considered in the present work? Moreover, is it possible to extend the bilayer model to reproduce the properties of the multilayer phase transitions for the open interfaces? These two points are discussed hereafter.

TABLE XI. Critical temperature T_c^p (in K) and critical bulk concentration $c_{trans}^p(T)$ at $T=300$, 600, and 900 K for $p\leqslant 2$ for the (001) surface, obtained with the monolayer model and with the complete calculations (values in parentheses).

	T_c^p	c_{trans}^p $T=300$ K	c_{trans}^p $T=600$ K	c_{trans}^p $T=900$ K
$p=0$	580(580)	1.7×10^{-11}	–	–
		(1.8×10^{-11})	–	–
$p=1$	1160(1500)	5.9×10^{-11}	7.7×10^{-6}	3.9×10^{-4}
		(6.1×10^{-11})	(7.9×10^{-6})	(4.1×10^{-4})
$p=2$	998(1100)	7.6×10^{-8}	2.7×10^{-4}	4.2×10^{-3}
		(7.3×10^{-8})	(2.8×10^{-4})	(4.1×10^{-3})

A. Application of the ground-state analysis

The simple Hamiltonian presented in Sec. V [see Eq. (8)] contains only two energetic parameters: $\Delta\tau$ and V. It predicts monolayer phase transitions for the (001) surface and a multilayer phase transition: $4\rightarrow6$ for the (310) surface, that does not depend on the energetic parameters. However, the isotherms shown in Sec. IV lead to the sequence $2\rightarrow5$ for the (310) surface. To analyze this discrepancy we determine the ground state of the Hamiltonian given by Eqs. (2)–(5), that contains much more energetic parameters: $\Delta H_p^{impurity}$ and $V_R^{p,p+p'}$ for all the pertinent values of p and p'. To this end, we calculate the internal energy of the system with n Ag-filled layers E_n as a function of the difference in chemical potentials $\mu=\mu_{Ag}-\mu_{Cu}$ in a way similar to the one in Eq. (9).

Figure 10 shows the ground states obtained from the lines $E_n(\mu)$ when the bulk is in the Ag-dilute solid solution ($\mu\leqslant\mu_c=\Sigma_R Z_R V_R=-372$ meV) for the three interfaces. We recover the sequence of monolayer phase transitions for the (001) surface [see Fig. 10(a)], in good agreement with the isotherms shown in Fig. 3 and the ground-state analysis of the simple Hamiltonian shown Fig. 9(a). For the (310) surface, we find the sequence $0\rightarrow1$, $1\rightarrow2$, $2\rightarrow5$, $5\rightarrow6$ [see Fig. 10(b)]. The multilayer phase transition $2\rightarrow5$ is in complete agreement with the results obtained at finite temperatures; see the isotherms shown Fig. 4. Moreover, the differences between the ground-states of the simple Hamiltonian [Eq. (8)] and the complete Hamiltonian [Eqs. (2)–(5)] indicate that the details of the multilayer phase transition, in particular the determination of the planes that participate in the transition, depend on the energetic parameters of the Hamiltonian. This contrasts with the multilayer character of the transition itself, that depends only on the crystallographic parameters within the simple model developed in Sec. V A. However, the subtle coupling between energetic and crystallographic parameters is illustrated by the following result: if the simple broken-bond model, [Eqs. (8) and (9)] is limited

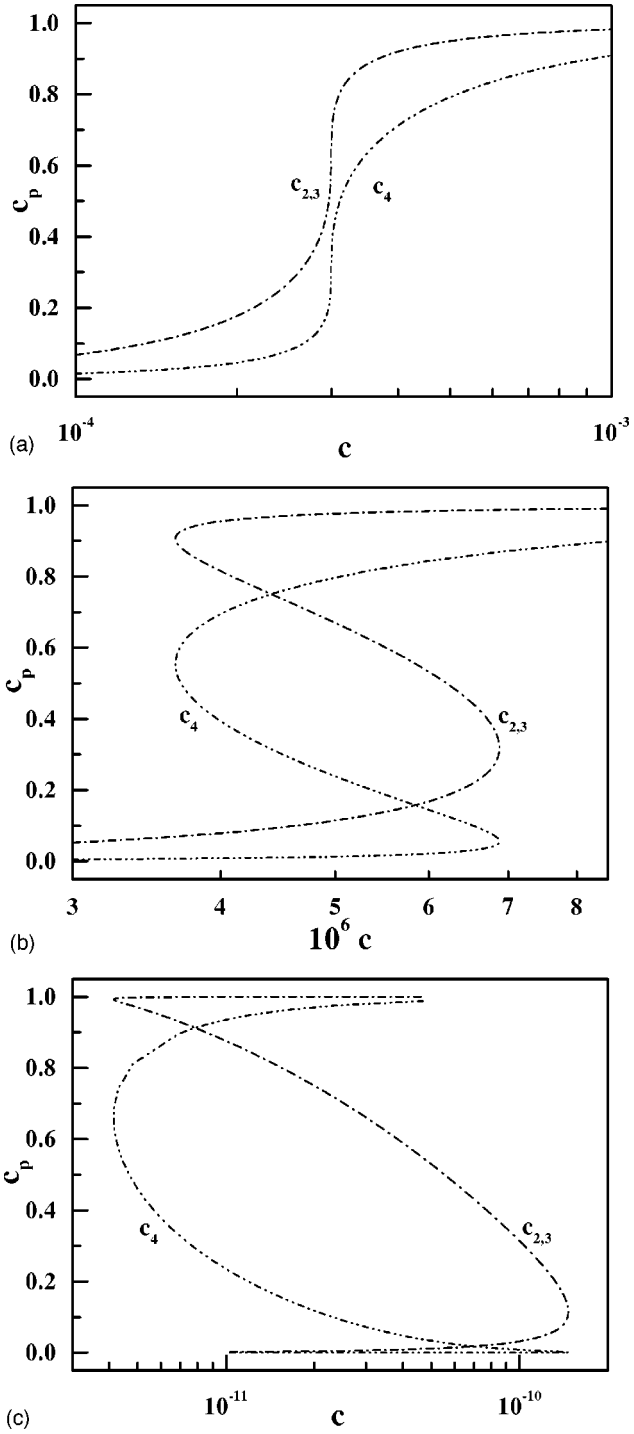

FIG. 11. Segregation isotherms for the (310) surface obtained in a bilayer model with $c_p=c_2=c_3$, $c_q=c_4$ at $T=900$ K (a), 600 K (b), and 300 K (c). In this simple model, it is assumed that $c_0=c_1=1$ and $c_{p'}=0$ for $p'>4$.

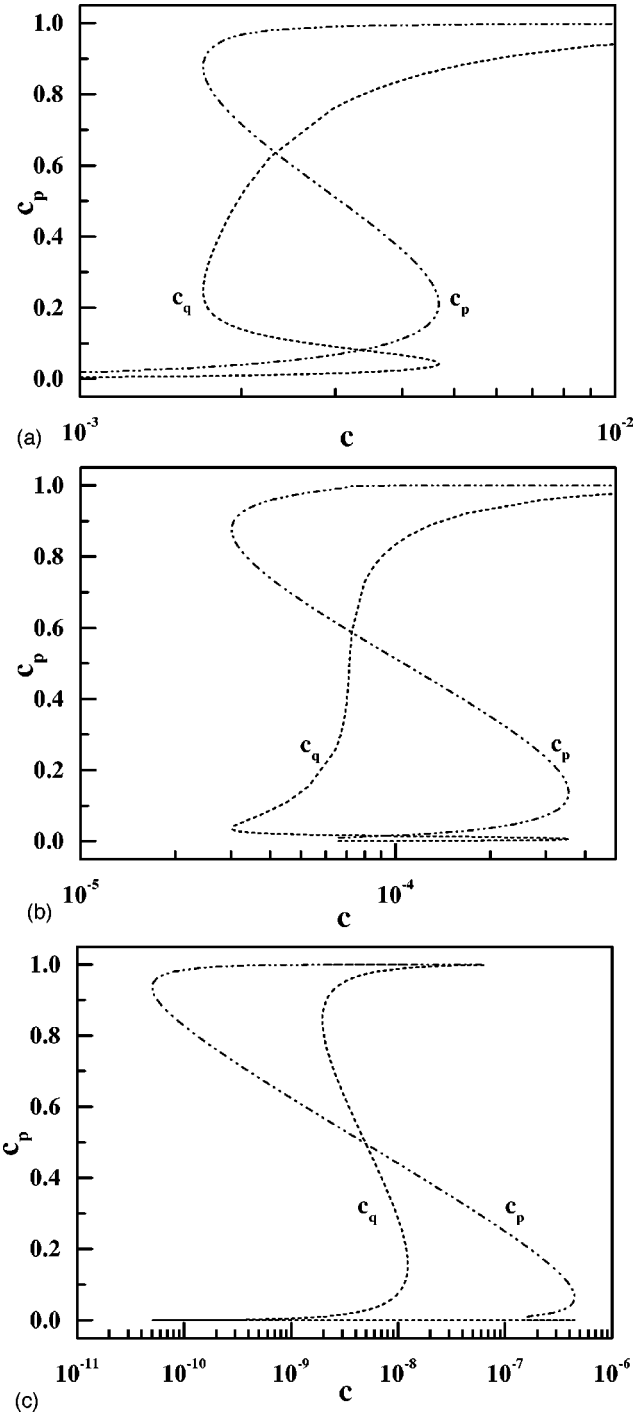

FIG. 12. Segregation isotherms for the $\Sigma=5$ (310) [001] tilt grain boundary obtained in a bilayer model with $c_p=c_0=c_{\pm 2}=c_{\pm 3}$, $c_q=c_{\pm 1}=c_{\pm 4}$ at $T=900$ K (a), 600 K (b), and 300 K (c). In this simple model, it is assumed that $c_{0'}=0$ and $c_{p'}=0$ for $p'>4$.

to nearest-neighbor interactions (instead of next-nearest neighbor interactions), a sequence of monolayer phase transitions (instead of the multilayer phase transition) is found for the (310) surface.

Finally, the study of the ground-states for the (310) [001] GB leads to the sequence $0\rightarrow 1$, $1\rightarrow 6$ [see Fig. 10(c)], where transition $1\rightarrow 6$ accounts for the jump of $c_{0'}$, $c_{\pm 1}$, $c_{\pm 2}$, $c_{\pm 3}$, $c_{\pm 4}$. Once more, this is in excellent agreement with the isotherms shown in Fig. 5, demonstrating the efficiency of the ground-state analysis.

B. Application of the monolayer-bilayer model

In this section, we analyze the ability of the monolayer and bilayer models to recover the main features of the inter-

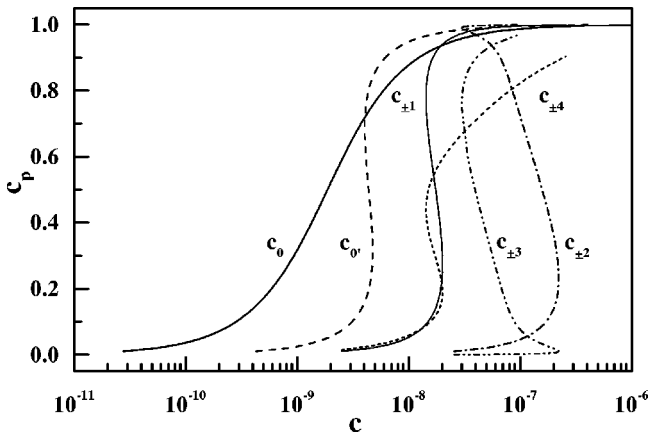

FIG. 13. Segregation isotherms for the $\Sigma=5$ (310) [001] tilt grain boundary at $T=300$ K obtained by considering simultaneously two bilayer models: B_{23} (for $c_{\pm2}$ and $c_{\pm3}$) and B_{14} (for $c_{\pm1}$ and $c_{\pm4}$) and two monolayer models: M_0 (for c_0) and $M_{0'}$ (for $c_{0'}$), see the text.

facial phase transitions. First we consider the (001) surface. In Table XI the values of T_c^p and c_{trans}^p, obtained with the monolayer model, are compared with the results issued from the complete calculation (see Sec. IV). The agreement is excellent and justifies fully the use of the monolayer model for the rather close-packed (001) surface. In particular the sequences $T_c^0<T_c^2<T_c^1$ and $c_{trans}^0<c_{trans}^1<c_{trans}^2$ are recovered. Note that the high value of T_c^1 is due to the large enhancement of $V_1^{1,1}$ (in absolute value) relative to the bulk value (see Table V).

Then, for the (310) surface, we solve the bilayer model with the assumptions. $c_p=c_2=c_3, c_q=c_4$ and $c_0=c_1=1, c_{p'}=0$ for $p'>4$, which are justified when considering the isotherms shown Fig. 4. The agreement between the resulting isotherms and the exact ones is very impressive (see Fig. 11). However, if the critical temperature given by the bilayer model, $T_c^{bilayer}=975$ K, is much higher than the one given by the monolayer model, $T_c^{monolayer}=270$ K, it remains lower than the exact one, $T_c=$ 1400 K. By successively considering a trilayer model (c_2,c_3,c_4) and a four-layer model (c_1,c_2,c_3,c_4), we find that the critical temperature of the trilayer model is very similar to $T_c^{bilayer}$, whereas the four layer model leads to a better estimation of T_c: 1100 K. This indicates how dependent on the various interlayer couplings the critical temperature is. This seems to exclude a quantitative analytical treatment of T_c for the multilayer phase transition, even if the bilayer model allows a very good description of the main features of the (310) surface segregation isotherms.

A similar analysis can be performed for the (310) GB isotherms. As explained in Sec. IV C, these segregation isotherms are more complex than for the (310) surface, in particular because of the influence of the vibrational entropy for the 0 sites. Thus if these sites do not participate in the multilayer phase transition at low temperature [see Fig. 5(d)], the lowering of the Gibbs free energy of segregation (in absolute value) due to ΔS_0^{seg} leads to the incorporation of the 0-site isotherm in this transition at high temperature, see Fig. 5(b). This must be taken into account in a simple bilayer model. In view of the isotherms shown Fig. 5(b), we adopt the generalized bilayer models: $c_p=c_0=c_{\pm2}=c_{\pm3}$, $c_q=c_{\pm1}=c_{\pm4}$ and $c_{0'}=c_{\pm p'}=0$ for $p'>4$. This leads to the isotherms shown Fig. 12 and to a critical temperature equal to 1650 K; [see Eq. (18)], in surprisingly good agreement with the numerical estimation given by the complete calculation, $T_c^{GB}\approx1600$ K (see Sec. IV C). This must be compared to the critical temperatures given by the monolayer model: from 58 K for the 0 sites to 400 K for the ±2 sites. This shows that the multilayer phase transition for the (310) GB has characteristics similar to the ones affecting the (310) surface. In both cases, the *interlayer* coupling is stronger than the *intralayer* one, contrary to the more studied case of the close-packed interfaces, such as the (001) surface.

An extension of the bilayer model can also be used to analyze the GB phase transition at low temperature. In Sec. IV C, we indicated that the GB phase transition is split into three phase transitions at $T=300$ K, the first one affecting the planes $p=\pm2$ and $p=\pm3$, the second one the planes $p=\pm1$ and $p=\pm4$, and the last one the sites $0'$ of the GB plane; see Fig. 5(d). This suggests the simultaneous use of two bilayer models, B_{23} and B_{14} and two monolayer models M_0 and $M_{0'}$. B_{23} is defined to study the phase transition for the planes ±2 and ±3 (i.e., $c_p=c_{\pm2}$ and $c_q=c_{\pm3}$ with $c_0=1$, $c_{0'}=c_{\pm1}=0$, $c_{p'}=0$ for $p'>3$), whereas B_{14} is devoted to the transition affecting the planes ±1 and ±4 (i.e., $c_p=c_{\pm1}$ and $c_q=c_{\pm4}$ with $c_0=c_{\pm2}=c_{\pm3}=1$, $c_{0'}=0$, and $c_{p'}=0$ for $p'>4$). The monolayer models, M_0 and $M_{0'}$ are used to study the behavior of the sites 0 ($c_p=c_0, c_{p'}=0$ for $p'>0$) and 0' ($c_p=c_{0'}, c_0=c_{\pm2}=c_{\pm3}=c_{\pm1}=c_{\pm4}=1$ and $c_{p'}=0$ for $p'>4$) of the GB plane, respectively.

Figure 13 displays the isotherms obtained with this simple method. They compare remarkably well with the complete calculation shown in Fig. 5(d). This allows us to understand the subtle succession of the three phase transitions. When increasing the bulk concentration, we first observe the continuous increase of c_0. All the other concentrations remain very small up to the phase transition affecting $c_{\pm2}$ and $c_{\pm3}$ for $c=c_{trans}^{2,3}$. However, for $c_{\pm2}$ and $c_{\pm3}$ almost equal to 1, a transition affecting $c_{\pm1}$ and $c_{\pm4}$ occurs for a value of c smaller than $c_{trans}^{2,3}$. This unusual situation explains the very large van der Waals loop affecting the $c_{\pm2}$ and $c_{\pm3}$ isotherms observed in the complete calculation, the transition for $c_{\pm1}$ and $c_{\pm4}$ being located in the upper and metastable part of this van der Waals loop [see Fig. 5(d)]. Moreover, this calculation confirms that the behavior of the $0'$ sites can be analyzed with the simple Fowler-Guggenheim isotherm,[25] the critical temperature obtained from the monolayer model (348 K), [see Eq. (14)], being in good agreement with the one estimated from the complete calculation (400 K).

Thus the bilayer model is a very efficient tool to analyze the complex interfacial multilayer phase transitions, when the interfacial plane is not a close-packed one. As shown for the (310) surface, the critical temperature is still approximate relative to the complete calculation, but this model allows to

understand the large increase of T_c relative to the widely used Fowler-Guggenheim (or monolayer) formalism.

VII. CONCLUSIONS

In this work, we have compared the segregation properties for three interfaces: the flat (001) surface, the open (310) surface and the $\Sigma=5$ (310) [001] GB. Using an *N*-body potential well suited for the Cu-Ag system, we have obtained the energetic parameters of an effective Ising model, which allows us to compare the segregation driving forces for the three interfaces. Within a mean-field approximation, we have calculated the segregation isotherms in the Cu-Ag system, which presents a strong tendency toward phase separation in the bulk. An interfacial phase transition occurs below a critical temperature in all the studied isotherms. However, if a succession of monolayer phase transitions is obtained for the (001) surface when approaching the bulk solubility limit, a very different behavior is exhibited for the two (310) interfaces. For these interfaces, we observe a multilayer phase transition affecting three planes for the (310) surface and nine planes for the (310) tilt GB. Moreover, a complex phase diagram is obtained for the GB plane itself, with the prediction of a multireentrant phase transition. An analysis of the ground-states allows us to define the condition for the existence of a multilayer phase transition relative to a monolayer one, as a function of the intra-layer and interlayer coordination numbers. Furthermore, the development of a simple bilayer model shows the influence of the interlayer coupling on the increase of the critical temperature relative to the estimation given by the well-known monolayer model (or Fowler-Guggenheim equation).

We hope that this study will motivate experimental works, particularly for the segregation properties of vicinal surfaces and GB in systems presenting a bulk miscibility gap, such as the Cu-Ag system. From the theoretical point of view, Monte Carlo simulations are in progress to study the influence of the correlations ignored by the present mean-field approach.

ACKNOWLEDGMENTS

It is a great pleasure to thank Guy Tréglia, Andrès Saúl, Döme Tanguy, and Jean-Marc Roussel for fruitful discussions.

[1] Y. Gauthier and R. Baudoing, in *Surface Segregation and Related Phenomena*, edited by P. A. Dowben and A. Miller (CRC Press, Boca Raton, FL, 1990), p. 169.
[2] S. M. Foiles and D. N. Seidman, in *Materials Interfaces: Atomic-level Structures and Properties*, edited by D. Wolf and S. Yip (Chapman & Hall, London, 1992), p. 497.
[3] G. Tréglia, B. Legrand, F. Ducastelle, A. Saúl, C. Gallis, I. Meunier, C. Mottet, and A. Senhaji, Comput. Mater. Sci. **15**, 196 (1999).
[4] R. W. Balluffi, in *Interfacial Segregation*, edited by W. C. Johnson and J. M. Blakely (ASM, Metals Park, OH, 1979), p. 193.
[5] L. Priester, J. Thibault, and V. Pontikis, Solid State Phenom. **59-60**, 1 (1998).
[6] E. D. Hondros, M. P. Seah, S. Hofmann, and P. Lejcek, in *Physical Metallurgy*, 4th ed., edited by R. W. Cahn and P. Haasen (North-Holland, Amsterdam, 1996), Vol. II, p. 856.
[7] D. N. Seidman, in *Materials Interfaces: Atomic-Level Structures and Properties* (Ref. 2), p. 58.
[8] Y. Kuk, P.J. Silverman, and T.M. Buck, Phys. Rev. B **36**, 3104 (1987).
[9] M. Schmidt, A. Biedermann, H. Stadler, and P. Varga, Phys. Rev. Lett. **69**, 925 (1992).
[10] D. Blavette, A. Bostel, J.M. Sarrau, B. Deconihout, and A. Menand, Nature (London) **363**, 432 (1993).
[11] F.L. Williams and D. Nason, Surf. Sci. **45**, 377 (1974).
[12] S. M. Foiles, in *Surface Segregation and Related Phenomena* (Ref. 1), p. 79.
[13] P. Wynblatt and R. C. Ku, in *Interfacial Segregation* (Ref. 4), p. 115.
[14] G. Tréglia and B. Legrand, Phys. Rev. B **35**, 4338 (1987).
[15] M. Guttmann, Metall. Trans. A **8**, 1383 (1977).
[16] C.L. White and W.A. Coglan, Metall. Trans. A **8**, 1403 (1977).
[17] C.L. White and D.F. Stein, Metall. Trans. A **9**, 13 (1978).
[18] A. Brokman, Acta Metall. **35**, 307 (1987).
[19] R. Kirchheim, Prog. Mater. Sci. **22**, 261 (1988).
[20] P. Lejcek and S. Hofmann, Crit. Rev. Solid State Mater. Sci. **20**, 1 (1995).
[21] S.M. Foiles, Phys. Rev. B **40**, 11 502 (1989).
[22] J.D. Rittner and D.N. Seidman, Acta Mater. **45**, 3191 (1997).
[23] D. Udler and D.N. Seidman, Acta Mater. **46**, 1221 (1998).
[24] D. Udler and D.N. Seidman, Interface Sci. **6**, 259 (1998).
[25] R. H. Fowler and E. H. Guggenheim, *Statistical Thermodynamics* (Cambridge University Press, Cambridge, 1960).
[26] G. Tréglia, B. Legrand, and F. Ducastelle, Europhys. Lett. **7**, 575 (1988).
[27] F. Berthier, B. Legrand, and G. Tréglia, Acta Mater. **47**, 2705 (1999).
[28] V. Rosato, M. Guillopé, and B. Legrand, Philos. Mag. A **59**, 321 (1989).
[29] G. Tréglia, B. Legrand, J. Eugène, B. Aufray, and F. Cabané, Phys. Rev. B **44**, 5842 (1991).
[30] C. Mottet, G. Tréglia, and B. Legrand, Phys. Rev. B **46**, 16 018 (1992).
[31] J. Eugène, B. Aufray, and F. Cabané, Surf. Sci. **273**, 372 (1992).
[32] Y. Liu and P. Wynblatt, Surf. Sci. **290**, 335 (1993).
[33] Y. Liu and P. Wynblatt, Surf. Sci. **310**, 27 (1994).
[34] A. Saúl, B. Legrand, and G. Tréglia, Phys. Rev. B **50**, 1912 (1994).
[35] A. Saúl, B. Legrand, and G. Tréglia, Surf. Sci. **331-333**, 805 (1995).
[36] A.P. Sutton and V. Vitek, Acta Metall. **30**, 2011 (1982).
[37] M. Menyhard, M. Yan, and V. Vitek, Acta Metall. Mater. **42**, 2783 (1994).
[38] F. Berthier, B. Legrand, G. Tréglia, and L. Priester, Mater. Sci. Forum **207-209**, 701 (1996).

[39] J. Creuze, F. Berthier, R. Tétot, B. Legrand, and D. Tanguy, Mater. Sci. Forum **294-296**, 423 (1999).
[40] J. Creuze, F. Berthier, R. Tétot, and B. Legrand, J. Phys. IV **9**, 51 (1999).
[41] J. Creuze, F. Berthier, R. Tétot, B. Legrand, and G. Tréglia, Phys. Rev. B **61**, 14 470 (2000).
[42] J. Creuze, F. Berthier, R. Tétot, and B. Legrand, Phys. Rev. B **62**, 2813 (2000).
[43] F. Ducastelle, *Order and Phase Stability in Alloys* (North-Holland, Amsterdam, 1991).
[44] A.V. Ruban and H.L. Skriver, Comput. Mater. Sci. **15**, 119 (1999).
[45] V. Drchal, A. Pasturel, R. Monnier, J. Kudrnovsky, and P. Weinberger, Comput. Mater. Sci. **15**, 144 (1999).
[46] I. Meunier, G. Tréglia, and B. Legrand, Surf. Sci. **441**, 225 (1999).
[47] J. Creuze, Thesis, Université Paris XI-Orsay, France 2000.
[48] C. H. Bennett, in *Diffusion in Solids, Recent Developments*, edited by A. S. Nowick and J. J. Burton (Academic, New York, 1975) p. 73.
[49] R. Haydock, V. Heine, and M.J. Kelly, J. Phys. C **5**, 2845 (1972).
[50] R. LeSar, R. Najafabadi, and D.J. Srolovitz, Phys. Rev. Lett. **63**, 624 (1989).
[51] A. A. Maradudin, E. W. Montroll, G. H. Weiss, and I. P. Ipavota, *Theory of Lattice Dynamics in the Harmonic Approximation*, (Academic, New York, 1971).
[52] G.J. Wang, A.P. Sutton, and V. Vitek, Acta Metall. **32**, 1093 (1984).
[53] Y. Teraoka and T. Seto, Surf. Sci. **255**, 209 (1991).
[54] J. Eugène, B. Aufray, and F. Cabané, Surf. Sci. **241**, 1 (1991).
[55] J. Du Plessis, Diffus. Defect Data, Pt. B **11**, 1 (1990).
[56] J.M. Roussel, A. Saúl, G. Tréglia, and B. Legrand, Phys. Rev. B **60**, 13 890 (1999).
[57] M. Lagües and J.L. Domange, Surf. Sci. **47**, 77 (1975).
[58] A. Patrykiejew, D.P. Landau, and K. Binder, Surf. Sci. **238**, 317 (1990).
[59] R. Pandit, M. Shick, and M. Wortis, Phys. Rev. B **26**, 5112 (1982).